Anthropogenic and climate-induced water storage dynamics in the China-Mongolia arid region adjacent to Altai Mountain over the past two decades

Yingjie Yan 1,2, Yuan Su 1,2, Siyu Wang1,2, Linlin Yao 3, Dashlkham Batmunkh 4 and Hongfei Zhou 1,*

1 Xinjiang Institute of Ecology and Geography, Chinese Academy of Sciences, Urumqi 830011, China;

2 University of Chinese Academy of Sciences, Beijing 100049, China;

3 College of Ecology, Environment and Resources, Guangdong University of Technology, Guangzhou 510006, China;

4 School of Engineering and Applied Sciences, National University of Mongolia, Ulaanbaatar 210646, Mongolia

*Correspondence: Hongfei Zhou (zhouhf@ms.xjb.ac.cn)

Contents of this file

Text S1 to S3

Figures S1 to S12

Table S1

Text S1 Uncertainty analysis

Previous studies indicate that variations among different GRACE solutions may result in discrepancies in TWSA trend estimates [1,2]. Hence, it is necessary to compare the three mascon products. The result showed that the trends in TWS derived from CSR-M, JPL-M and GSFC-M show good consistency (Fig. S5, Fig. S6). During the study period, the three mascon solutions consistently exhibited a positive TWSA trend over the study area, with the change rates of -0.42 ± 0.02 cm/yr ($p < 0.01$) for CSR Mascon, -0.50 ± 0.02 cm/yr ($p < 0.01$) for JPL Mascon, and -0.48 ± 0.02 cm/yr ($p < 0.01$) for GFZ_Mascon, respectively (Fig. S7). The uncertainty due to different data sources can be reduced by taking the ensemble mean of three mascon solutions [3–5]. Therefore, the ensemble mean of JPL-M, CSR-M, GSFC-M was used to represent the TWS in the ACM.

Similarly, the uncertainties in the GLDAS datasets are caused by limited input datasets and an inability to accurately model complex hydrological processes [6,7]. Since GWS is obtained by subtracting GLDAS TWS from GRACE TWS, which may increase the uncertainty in GWS estimates due to the accumulation of uncertainties of each component storage [5,8]. Therefore, to reduce uncertainty, we employed the ensemble mean of multiple models.

In addition, the comparison of GLDAS LSM components reveals that the variability of the canopy water storage component is negligible (Fig. S1), so was not considered when separating the groundwater storage component. Another limitation originates from the interference of mass loss due to extraction of mineral resources on the equivalent water height, which may overestimate the variations of TWS given that GRACE derives the TWS changes based on the Earth's gravitational change. It is difficult to obtain long time series spatiotemporal data sets for mineral resource extraction, which do not well help us understand the spatiotemporal variation of TWS on the monthly scale. Although the impact of mineral resource extraction on TWS trends is limited, deducting its effects could improve the estimations of the seasonal variations in TWS.

The trends in water reserve components derived from Noah, VIC, CLSM_OL and CLSM_DA show good consistency. However, the differences in the processing and methodology of Noah, VIC, CLSM_OL and CLSM_DA to derived water reserve components result in the uncertainties of results[9]. The uncertainty of water reserve components can be obtained by calculating the standard deviation of the four LSMs. Figure S2 shows the spatial distribution of SWSA, SWEA, and SMSA uncertainty. It can be seen that the areas with high uncertainty in SWSA are mainly located in the lower reaches of the URB in JBNWC, those in SWEA are mainly located in the middle of the KRB in GLDWM, and those in SMSA are mainly located in the western part of the NTRB in JBNWC, as well as a small part of the middle of the Gurbantunggut in JBNWC. The probability density function (PDF) plot shows that the uncertainty of SWSA trend varies from 0.03 mm/yr to 1.63 mm/yr, with a mean value of 0.35 mm/yr and a median value of 0.3 mm/yr. The uncertainty of SWEA trend varies from 0.04 mm/yr to 0.88 mm/yr, with a mean value of 0.38 mm/yr and a median value of 0.34 mm/yr. And those of SMSA trend varies from 0.0004 mm/yr to 8.6 mm/yr, with a mean value of 1.39 mm/yr and a median value of 0.83 mm/yr. Previous studies have shown that the uncertainty due to different data sources can be reduced by taking the ensemble mean of four LSMs [10–12]. Therefore, the ensemble mean of Noah, VIC, CLSM_OL and CLSM_DA was used to represent the water reserve components in CMA.

Text S2 The GRACE-derived GWSA was validated through comparison with groundwater well observations.

Due to the difficulty in obtaining in-situ groundwater table data in the Great Lakes region of western Mongolia, this paper qualitatively compares in-situ groundwater table data in the Junggar Basin of Northwest China with downscaling GWSA results. Notably, in calculating the RMSE, the time series is normalized due to the magnitude difference between the in-situ level and the downscaling results. For 0.5° original GWSA retrieved by GRACE, the overall CC and RMSE are 0.364 and 0.093, respectively, compared with in-situ groundwater table measurements, while the overall CC and RMSE are 0.437 and 0.087, respectively, for 0.1° GWSA after deviation correction downscaling (FIG. S8b and FIG. S8d). Therefore, downscaling models combined with residual-corrected random forest regression can better replicate long-term trends and seasonal changes observed in situ. Compared with the original results, the correlation coefficient has been significantly improved, increasing by 19.72%. A similar downscaling improvement can be observed for the RMSE index, as shown in Figure 10c-d.

Text S3 EOF analysis.

Since snow water, glacier meltwater, soil moisture, surface water and groundwater affect TWSA (with canopy water being negligible in the CMA (Figure S2)), we estimated each component's contribution to TWSA in the Junggar Basin of Northwestern China (JBNWC) and the Great Lakes Depression region of western Mongolia (GLDWM) regions separately. In both the JBNWC and GLDWM, GWSA is the primary contributor to TWSA variance, accounting for 78.16% and 90.28%, respectively, followed by SWEA at 18.61% and 6.04%. This indicates that TWSA variation is largely driven by fluctuations in groundwater reserves. Therefore, to record effective signals and extract valuable information from our research results, we have used EOF analysis to explore the spatiotemporal patterns of TWSA, GWSA, and PME (precipitation minus evapotranspiration) in the JBNWC and the GLDWM respectively. For JBNWC, the EOF components of the TWSA indicated that 82.57% and 9.13% of the variation in TWSA can be explained by the EOF1 and EOF2, respectively. The similarity of EOF1 in spatial patterns between TWSA and GWSA indicated that the EOF1 represented anthropogenic GWSA (Figure.S11a and 11c). The sharply declining trend of both PC1, consistent with the TWSA trend, further confirmed this conclusion (Figure.S11e). The insignificant increasing patterns in the spatial dimension (EOF2) and temporal dimension (PC2) were consistent with net precipitation (PME), suggesting that EOF2 could be regarded as natural TWSA. For GLDWM, the EOF components of the TWSA indicated that 63.59% and 13.93% of the variation in TWSA can be explained by the EOF1 and EOF2, respectively. The similarity of EOF1 in spatial patterns between TWSA and net precipitation (PME) indicated that the EOF1 represented natural TWSA (Figure.S12a and 12c). The variation trends of both PC1s are consistent with the TWSA trend, further confirming this conclusion (Fig. S12e). The insignificant increasing patterns in the spatial dimension (EOF2) and temporal dimension (PC2) were consistent with GWSA, suggesting that EOF2 could be regarded as anthropogenic TWSA. As described above, natural TWSA is associated with net precipitation (PME), representing the influence of natural hydrological processes, and can be quantified by the inter-annual items of the TWSA. The seasonal cycle also influences natural TWSA, as precipitation, evapotranspiration, and runoff exhibited distinct seasonal variations. The linear trend and sub-seasonal residuals were related to anthropogenic TWSA, as human activities have a dramatic and irregular effect on TWS. Therefore, in this study, we defined the inter-annual and seasonal items of the TWSA as the natural TWSA, and the linear trend and sub-seasonal residuals of the TWSA as the anthropogenic TWSA, based on the STL and EOF analysis.

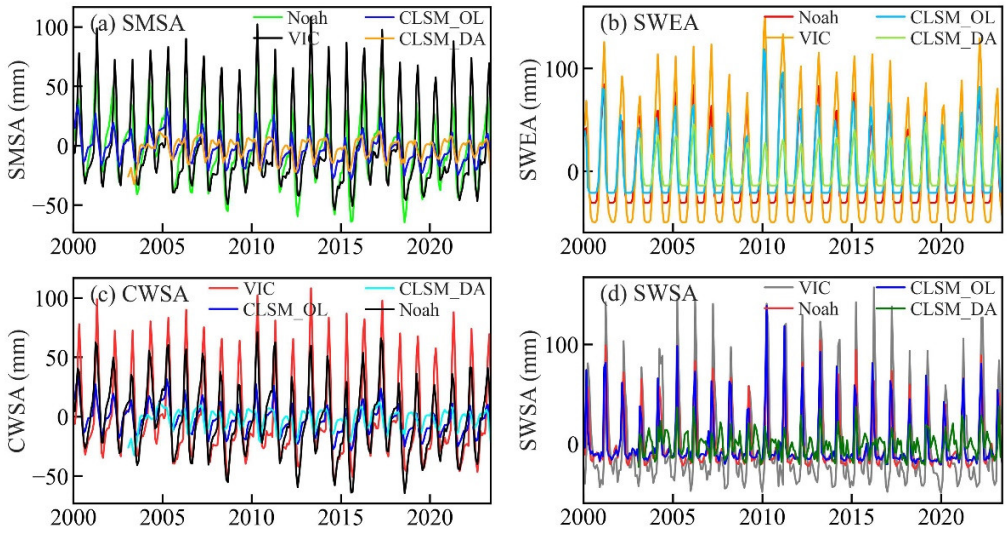


Figure.S1 The temporal variations of terrestrial water storage components from Noah LSM, VIC LSM and CLSM LSM: (a) SMSA; (b) SWEA; (c) CWSA; (d) SWSA.

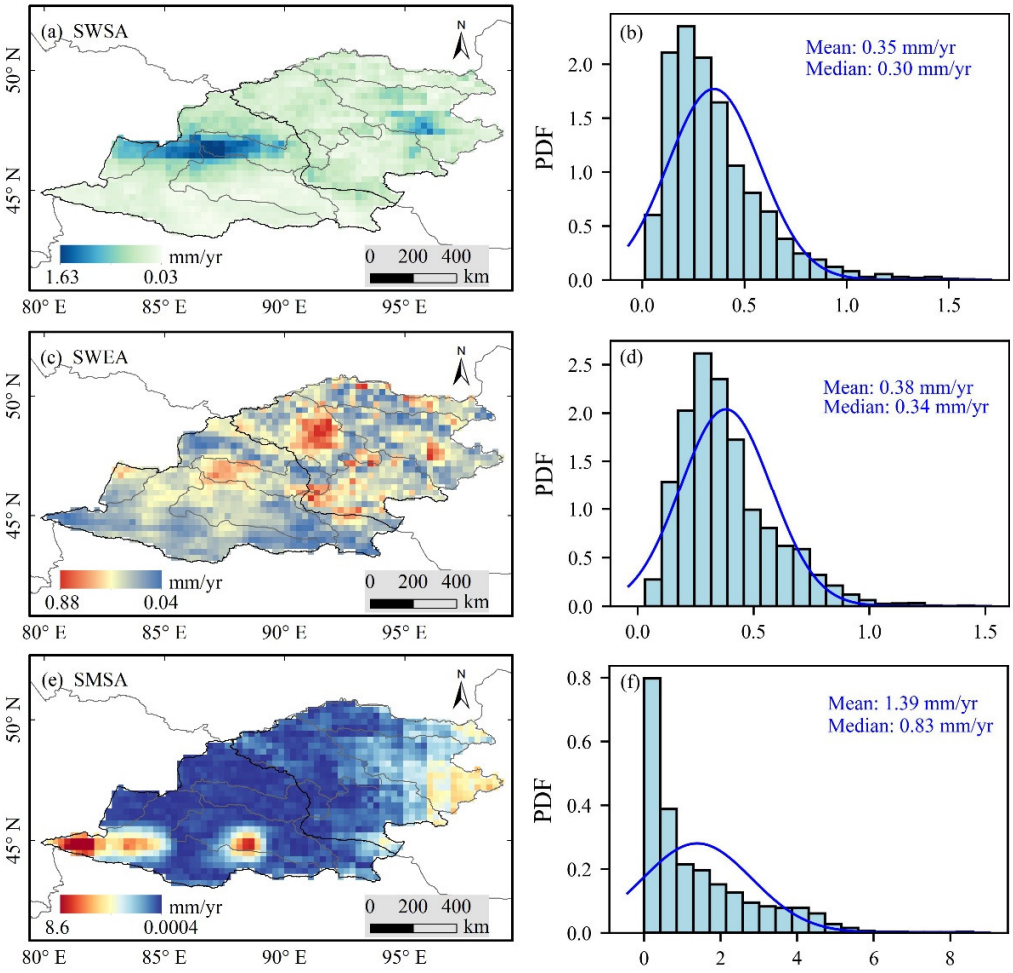


Figure.S2 Spatial distribution (left panel) and the PDF (right panel) of LSM uncertainty.

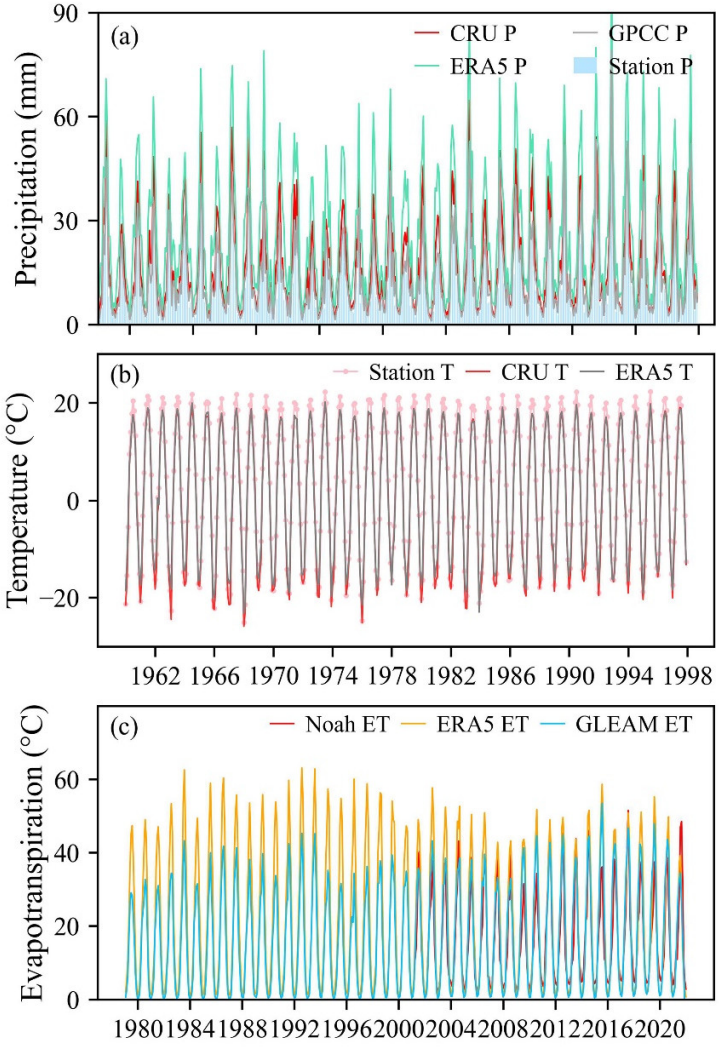


Figure.S3 Multi-sources climate variables: (a) precipitation data from the mean of NOAA's Climate Data Online (CDO), Climate Research Unit gridded Time Series (CRU TS) datasets, ERA5-Land reanalysis datasets, and GPCC satellite datasets; (b) temperature (i.e., 2m temperature) data from NOAA's Climate Data Online (CDO), ERA5-Land reanalysis datasets and Climate Research Unit gridded Time Series (CRU TS) datasets; (c) evapotranspiration data from Noah LSM, ERA5-Land reanalysis datasets and GLEAM dataset.

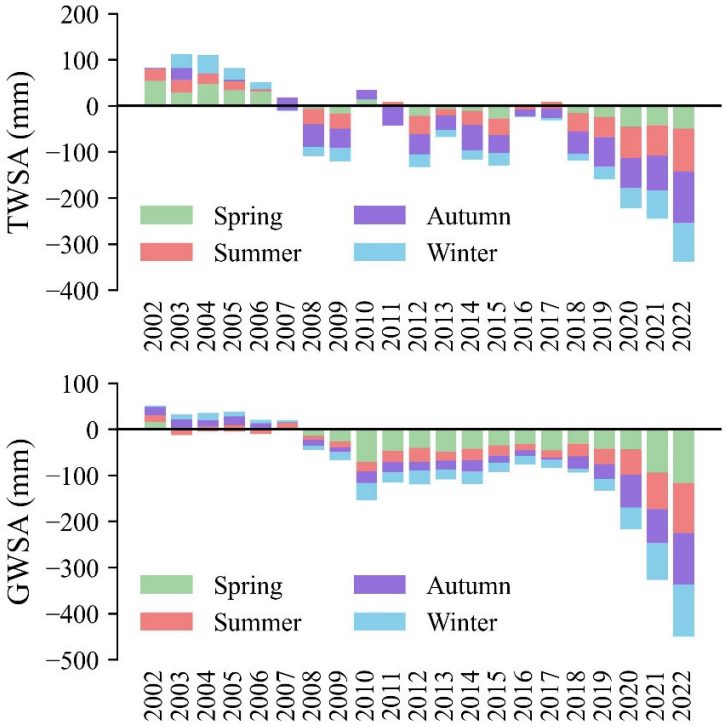


Figure.S4 The seasonal variation characteristics of terrestrial water storage anomaly during 2002–2023.

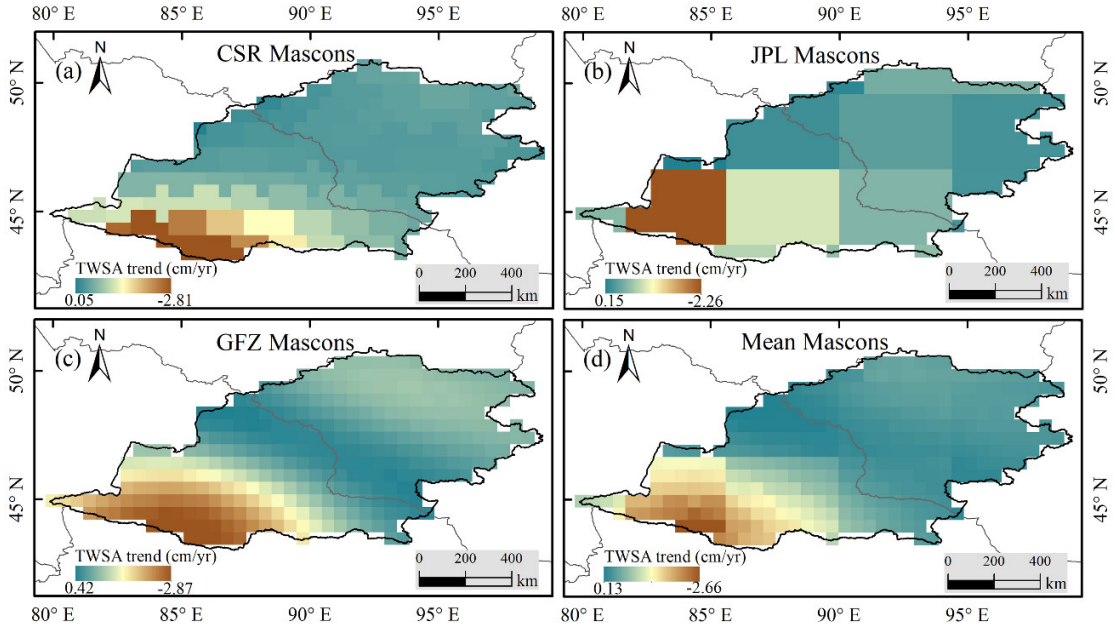


Figure.S5 Spatial distributions of annual total water storage anomaly (TWSA) trends from (a) CSR mascon (CSR-M), (b) JPL mascon (JPL-M), (c) GSFC mascon (GSFC-M) and (d) the mean of CSR-M, JPL-M and GSFC-M.

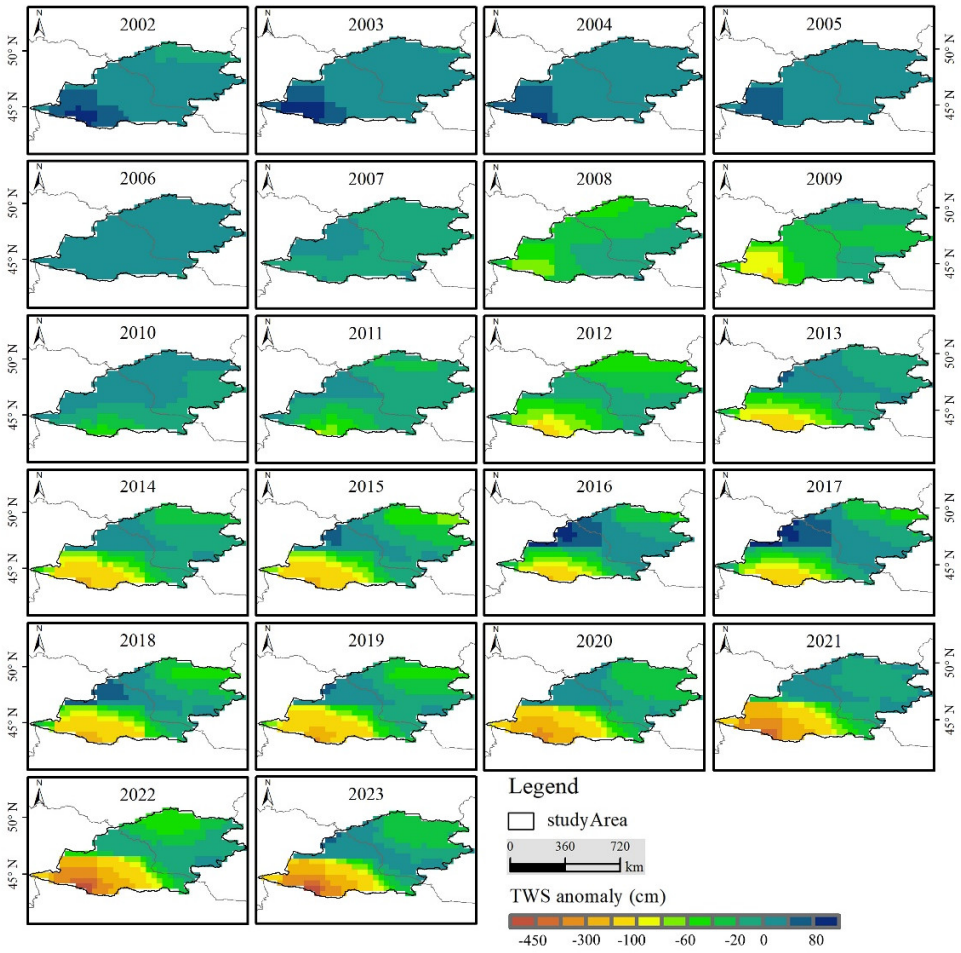


Figure.S6 Spatial evolution of annual average total water storage anomalies (TWSA) (the ensemble mean of TWSA from CSR-M, JPL-M and GSFC-M) for the period of 2002-2023 from GRACE and GRACE-FO satellite missions.

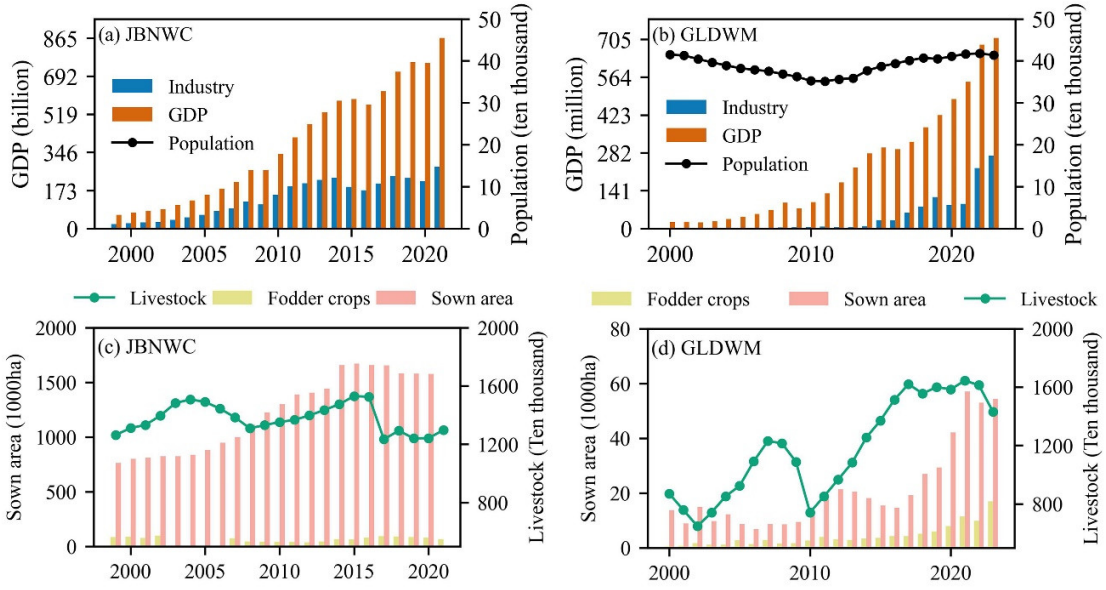


Figure.S7 Changes in population, GDP, industry, sown area and number of livestock in Xinjiang and Mongolia from 2000 to 2021.

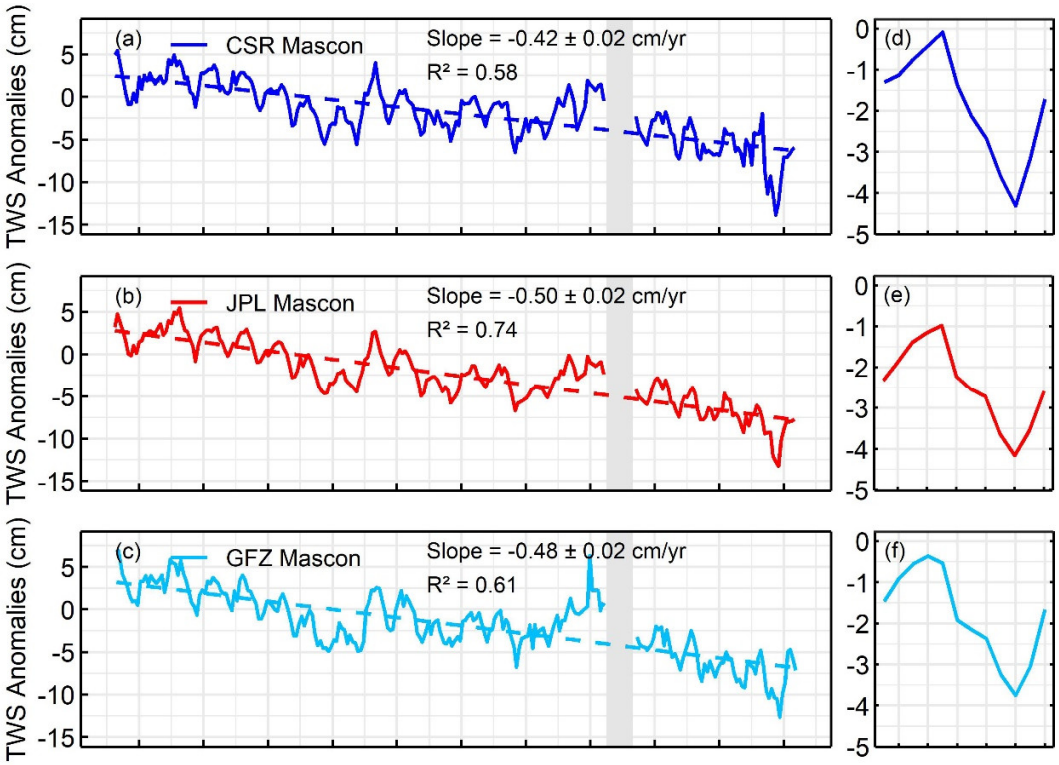


Figure.S8 Spatially averaged monthly total water storage (TWS) anomalies derived from (a) CSR mascon (CSR-M), (b) JPL mascon (JPL-M), (c) GFZ mascon (GFZ -M). The dashed straight line represents the linear fitting, and the gray shading represents the gap between GRACE and GRACE-FO. (d)-(f) represent the monthly average of CSR-M, JPL-M and GFZ -M, respectively.

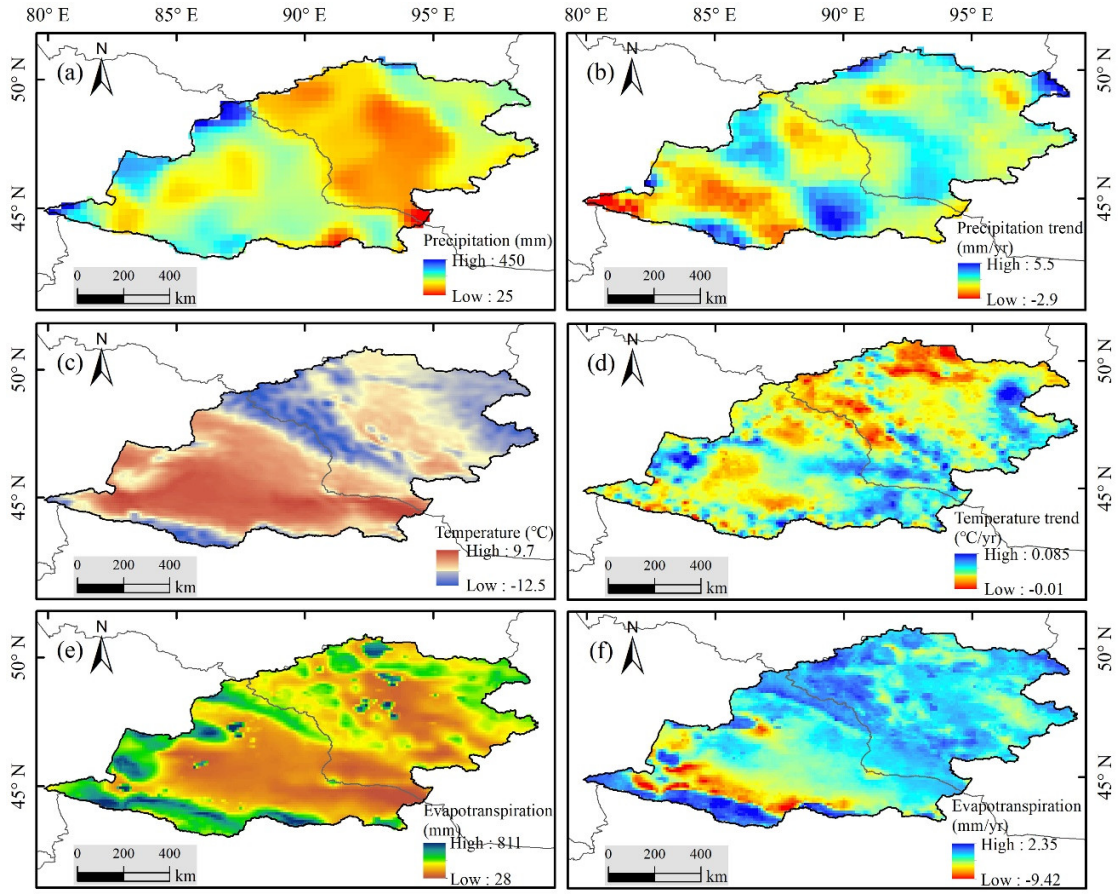


Figure.S9 Spatial distribution of annual average (a) precipitation, (c) temperature, (e) evapotranspiration in the period of 2000-2023. The interannual trends of (b) precipitation, (d) temperature, (f) evapotranspiration during 2000-2023. The three climate variables are derived from ERA5-Land reanalysis dataset.

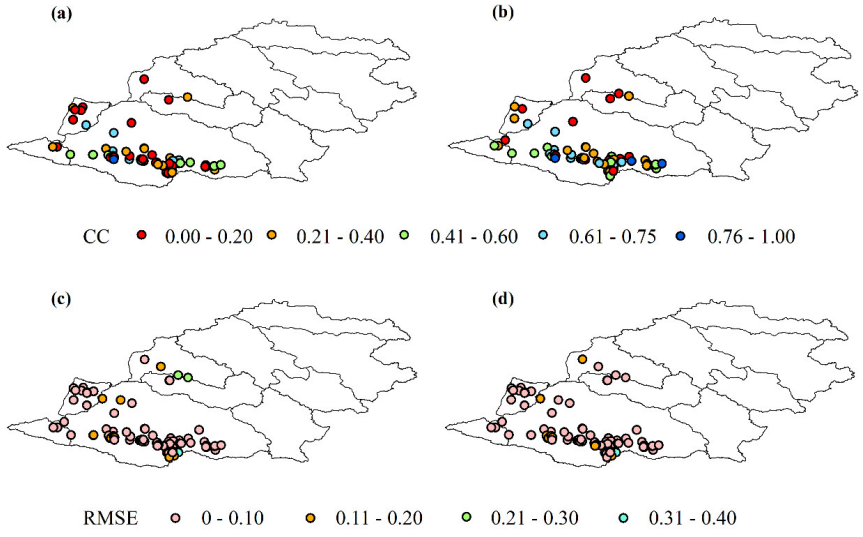


Figure.S10 Comparisons of GWS anomaly derived from GRACE and groundwater level anomaly.

Table S1 Climatic and anthropogenic contributions on TWSA for the period 2002–2023 and subperiods 2002–2010 and 2011–2023

Region	Time	Climate change-induced (%)		Human-induced (%)	
		Positive	Negative	Positive	Negative
JBNWC	2002-2010	44.19	-54. 12	57.91	-31.91
	2011-2023	31.44	-26.54		-70.67
	2002-2023	35.92	-39.77	57.91	-63.99
GLDWM	2002-2010	58.94	-67.70	44.07	-25.18
	2011-2023	40.85	-43.80	29.66	-58.52
	2002-2023	48.49	-53.44	43.25	-51.45

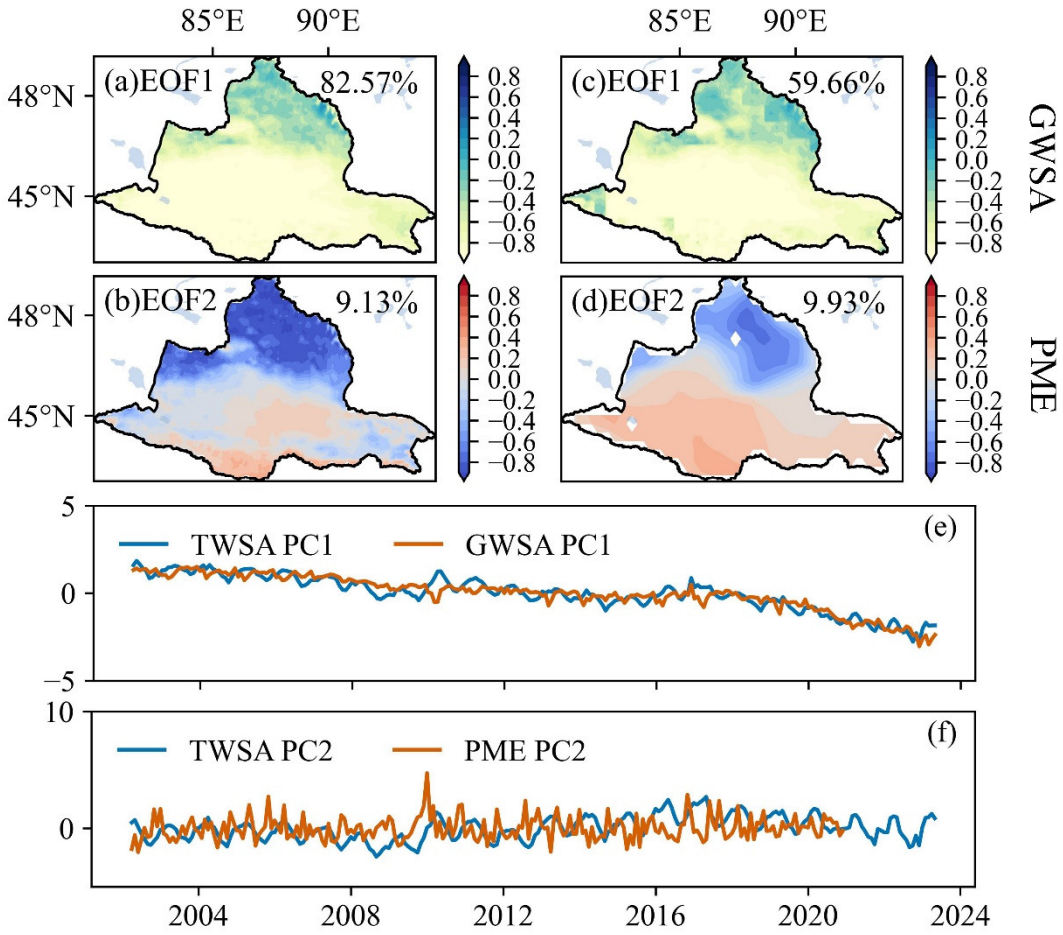


Figure.S11 (a), (b), (c), (d) spatial patterns and (e), (f) corresponding temporal patterns of TWS, GWS and PME in the Junggar Basin of Northwestern China (JBNWC).

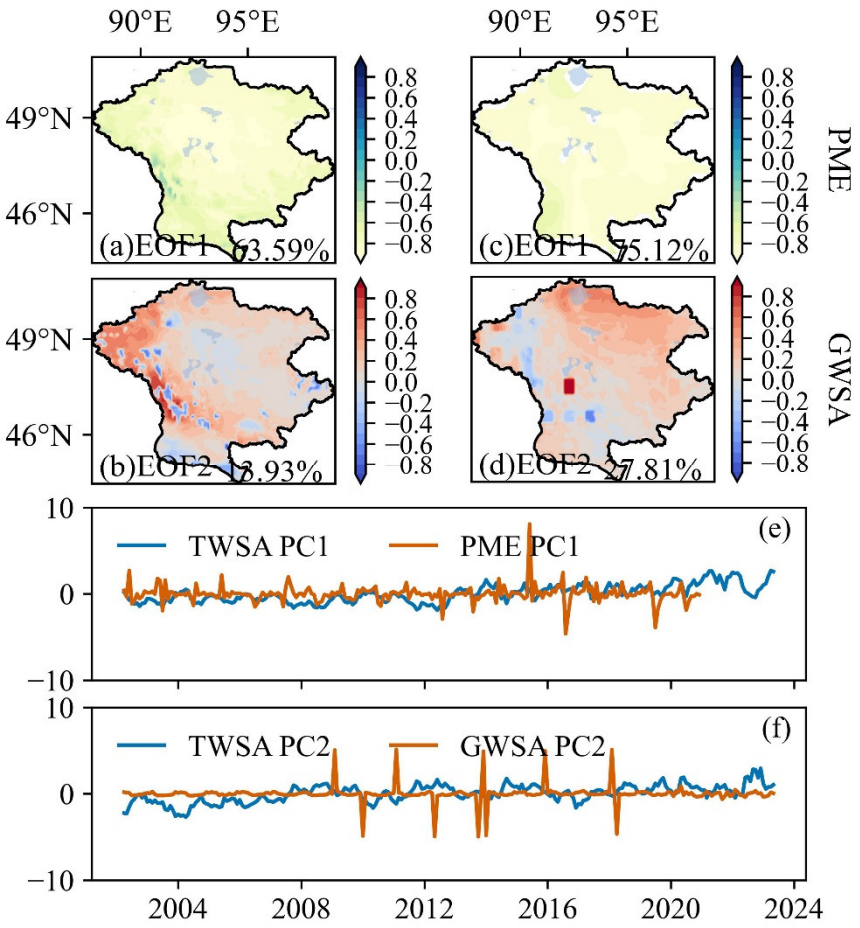


Figure.S12 (a), (b), (c), (d) spatial patterns and (e), (f) corresponding temporal patterns of TWS, GWS and PME in the Great Lakes Depression region of western Mongolia (GLDWM).

Reference

1. Jing, W.; Yao, L.; Zhao, X.; Zhang, P.; Liu, Y.; Xia, X.; Song, J.; Yang, J.; Li, Y.; Zhou, C. Understanding Terrestrial Water Storage Declining Trends in the Yellow River Basin. *J. Geophys. Res.: Atmos.* **2019**, *124*, 12963–12984, doi:10.1029/2019JD031432.

2. Scanlon, B.R.; Zhang, Z.; Save, H.; Wiese, D.N.; Landerer, F.W.; Long, D.; Longuevergne, L.; Chen, J. Global Evaluation of New GRACE Mascon Products for Hydrologic Applications. *Water Resour. Res.* **2016**, *52*, 9412–9429, doi:10.1002/2016WR019494.

3. Bhanja, S.N.; Zhang, X.; Wang, J. Estimating Long-Term Groundwater Storage and Its Controlling Factors in Alberta, Canada. *Hydrol. Earth Syst. Sci.* **2018**, *22*, 6241–6255, doi:10.5194/hess-22-6241-2018.

4. Chang, L.; Yuan, R.; Gupta, H.V.; Winter, C.L.; Niu, G. Why Is the Terrestrial Water

Storage in Dryland Regions Declining? A Perspective Based on Gravity Recovery and Climate Experiment Satellite Observations and Noah Land Surface Model with Multiparameterization Schemes Model Simulations. *Water Resour. Res.* **2020**, *56*, e2020WR027102, doi:10.1029/2020WR027102.

5. Zou, Y.; Kuang, X.; Feng, Y.; Jiao, J.J.; Liu, J.; Wang, C.; Fan, L.; Wang, Q.; Chen, J.; Ji, F.; et al. Solid Water Melt Dominates the Increase of Total Groundwater Storage in the Tibetan Plateau. *Geophys. Res. Lett.* **2022**, *49*, e2022GL100092, doi:10.1029/2022GL100092.

6. Scanlon, B.R.; Zhang, Z.; Save, H.; Sun, A.Y.; Müller Schmied, H.; Van Beek, L.P.H.; Wiese, D.N.; Wada, Y.; Long, D.; Reedy, R.C.; et al. Global Models Underestimate Large Decadal Declining and Rising Water Storage Trends Relative to GRACE Satellite Data. *Proc. Natl. Acad. Sci.* **2018**, *115*, doi:10.1073/pnas.1704665115.

7. Hu, Z.; Zhou, Q.; Chen, X.; Chen, D.; Li, J.; Guo, M.; Yin, G.; Duan, Z. Groundwater Depletion Estimated from GRACE: A Challenge of Sustainable Development in an Arid Region of Central Asia. *Remote Sensing* **2019**, *11*, 1908, doi:10.3390/rs11161908.

8. Rateb, A.; Scanlon, B.R.; Pool, D.R.; Sun, A.; Zhang, Z.; Chen, J.; Clark, B.; Faunt, C.C.; Haugh, C.J.; Hill, M.; et al. Comparison of Groundwater Storage Changes from GRACE Satellites with Monitoring and Modeling of Major U.S. Aquifers. *Water Resources Research* **2020**, *56*, e2020WR027556, doi:10.1029/2020WR027556.

9. Qi, W.; Liu, J.; Yang, H.; Zhu, X.; Tian, Y.; Jiang, X.; Huang, X.; Feng, L. Large Uncertainties in Runoff Estimations of GLDAS Versions 2.0 and 2.1 in China. *Earth Space Sci.*

10. Xiong, J.; Guo, S.; Abhishek; Chen, J.; Yin, J. Global Evaluation of the "Dry Gets Drier, and Wet Gets Wetter" Paradigm from a Terrestrial Water Storage Change Perspective. *Hydrol. Earth Syst. Sci.* **2022**, *26*, 6457–6476, doi:10.5194/hess-26-6457-2022.

11. Xie, Z.; Wang, L.; Wang, Y.; Liu, B.; Li, R.; Xie, J.; Zeng, Y.; Liu, S.; Gao, J.; Chen, S.; et al. Land Surface Model CAS-LSM: Model Description and Evaluation. *JAMES* **2020**, *12*, e2020MS002339, doi:10.1029/2020MS002339.

12. Liu, Y.; Yang, Z.; Lin, P.; Zheng, Z.; Xie, S. Comparison and Evaluation of Multiple Land Surface Products for the Water Budget in the Yellow River Basin. *J. Hydrol.* **2020**, *584*, 124534, doi:10.1016/j.jhydrol.2019.124534.